Materials and Structures (2019) 52:89
https://doi.org/10.1617/s11527-019-1389-y

ORIGINAL ARTICLE

Probabilistic identification of the effects of corrosion propagation on reinforced concrete structures via deflection and crack width measurements

Louise Bichara · George Saad · Wael Slika

Received: 18 March 2019 / Accepted: 13 August 2019 / Published online: 17 August 2019

Abstract This study presents a probabilistic framework for accurate prediction of the impacts of corrosion propagation on reinforced concrete (RC) structures. The presented framework uses the ensemble Kalman filter (EnKF) coupled with easily acquired measurements of corrosive crack widths and mid-span deflection increases for identifying and calibrating corrosion propagation models. The calibrated models are consequently used to forecast the extent of corrosion propagation in RC structures. To assess the efficacy of the presented framework, data corresponding to the long-term chloride-induced corrosion experiments initiated in 1984 at "Laboratoire des Materiaux et Durabilite des Constructions" (L.M.D.C.) in Toulouse, south-west France are used. The results accentuate the robustness of the presented EnKF approach by being able to identify and calibrate candidate corrosion propagation models capable of predicting, with reasonable accuracy, the experimental measurements of corrosive crack width and mid-span deflection in RC members.

L. Bichara · G. Saad (✉)
Department of Civil and Environmental Engineering, American University of Beirut, P.O. Box 11-0236, Riad El Solh, Beirut 1107, Lebanon
e-mail: george.saad@aub.edu.lb

W. Slika
Department of Civil and Environmental Engineering, Beirut Arab University, Debbieh, Lebanon

Keywords Corrosion propagation rate · Reinforced concrete · Ensemble Kalman filter · Data assimilation · Uncertainty quantification

1 Introduction

Corrosion of the reinforcing steel bars is one of the main causes for premature deterioration and failure of reinforced concrete (RC) structures [1]. Neglecting the problem of corrosion in RC structures could lead to sudden damages and consequently resulting in significant repair costs and endangering public safety. In fact, according to studies in the United States, the direct cost of corrosion is a shocking $276 billion on an annual basis [2].

Corrosion of RC structures is regarded as a two stages process: the initiation stage and the propagation stage [3]. Initially, the high alkaline nature of concrete (pH > 13.5) [1] forms a protective film around the embedded steel bars. This protective layer prevents the oxidation of steel from occurring. Corrosion is typically triggered by the presence of chloride ions and/or carbonation agents in the surrounding environment. These agents tend to reduce the pH of the concrete and consequently lead to the loss of the protective film and the initiation of the corrosion. Therefore, the initiation phase is the time required for the de-passivation agents diffusing into the concrete and accumulating at the rebar level to reach a certain threshold value after which the passive layer of the reinforcement is permanently altered and corrosion is activated [4]. During the propagation phase, rust products form on the rebar surface due to the electrochemical process of the dissolution and transformation of metal ions on the steel bar surface into rust [5]. Since the rust products occupy a bigger volume than that of the steel [6], volumetric expansion causes losses in the rebar area, leading to damage in the concrete in the form of cracking, destruction of cover and loss of bond between the concrete and the steel [1, 7–9]. Therefore, as corrosion progresses, it degrades the resistance capacity of the structure and decreases the design safety margin. Proper gauging of the corrosion propagation rate is highly critical as it allows for estimating the remaining service life of the structure.

There exist different studies in the literature concerning monitoring the corrosion propagation rate using non-destructive tests. Such tests include infrared thermography [10–12] and X-ray imaging [13–15] for determining the steel cross-section loss; and the linear polarization resistance technique (LPR) [16, 17] for measuring the rate of corrosion. However, these tests are costly in nature and not easily implemented in situ. To overcome these difficulties, many researchers worked on developing empirical prediction models to simulate the extent of damage during the corrosion propagation phase such as: Liu and Weyers model [18], Yalcyn and Ergun model [19], Vu and Stewart model [20, 21], Alonso et al.'s model [22], Scott's model [23], Breysse et al. model [24], Li model [25]. In all these models, the main factor which governs the deterioration process during corrosion propagation is the corrosion rate which is typically represented as an electric current [5].

A limitation of the empirical models available in the literature is their inability to quantify the uncertainties underlying the corrosion propagation process. These uncertainties can be attributed to several sources including mathematical modeling simplifications, non-homogeneity of concrete and consequently the stochastic nature of the model parameters, and uncertain environmental conditions that might either slow or accelerate the corrosion propagation process. To increase confidence in these empirical models, practitioners recommend continuous monitoring of the structural response under changing environmental conditions to avoid the risks associated with catastrophic failures. Using compiled experimental data, Faroz et al. [26] presented a Bayesian approach for the corrosion reliability analysis of reinforced concrete components. However, the data used in Faroz et al.'s study was gathered for a short time period spanning few months only. Hackl [27] used a combination of structural reliability analysis and Bayesian networks and presented a framework for the stochastic modeling of reinforced concrete deterioration caused by corrosion. In his study, Hackl used the Half Cell Potential Method to track the progress of corrosion and consequently update the probability of failure of RC structures. The problem with most of the cases presented in the literature is the fact that the corrosion data used for updating did not span naturally for a long period of time, and that the non-destructive testing mechanisms used were costly and not easily implementable.

In an attempt to overcome these deficiencies, this study presents a probabilistic framework that uses the ensemble Kalman filter (EnKF) to calibrate the governing parameters of corrosion propagation models by simply monitoring measurable, non-costly and non-destructively tested aspects of corrosion, namely deflection and crack width opening. The calibrated models can be used for simulating corrosion in RC structures and for reliability analysis at different stages during the remaining life of these structures. The EnKF is a sequential data assimilation tool which relies on the Monte Carlo methods to forecast the error statistics [28]. The use of the EnKF was successfully demonstrated by the authors for estimating the corrosion initiation time in previous studies [4].

To validate the presented SHM framework, it is applied to an ongoing program of long-term chloride-induced corrosion experiments that was initiated in 1984 at "Laboratoire des Materiaux et Durabilite des Constructions" (L.M.D.C.) in Toulouse, south-west France. Data points pertinent to both deflection and crack width were gathered [29–31] from two beams under constant supervision for a long period of time: 23 year old B2Cl1 [30] and 26 year old B2Cl2 [31]. The gathered data is first used to calibrate the model parameters of existing corrosion propagation models. Then, the calibrated models are used for predicting the future behavior of the RC corroded structures.

2 Corrosion propagation

The corrosion propagation phase is mainly governed by the corrosion propagation rate, a current which transforms the iron metal into rust thus leading to the degradation of the steel properties. Since rust occupies a volume greater than that of steel, volumetric expansion around the rebar will also lead to the cracking of the surrounding concrete [32].

Several models were developed in the literature to simulate the corrosion propagation rate. Table 1 below summarizes some of these corrosion rate propagation models while listing the advantages and disadvantages of each. It is to be noted that the presented corrosion rate propagation models follow one of three possible trends; they either remain stationary, decrease or increase with time. Moreover, these different models rely on governing environmental and loading conditions, quality of concrete mix, and cross-section geometry to simulate the corrosion propagation rate in RC structures. However, most of the models only account for the aforementioned conditions in estimating the initial corrosion rate. The corrosion rate is then empirically propagated in time via fitting experimental data to either polynomial or exponential expressions. Furthermore, none of the models presented in the literature has been applied to real-time structures where corrosion propagation is naturally induced and spans for a long period of time. In fact, most of the data used for developing these

Table 1 Corrosion propagation rate models in the literature: formulation, pros and cons, time-variation trend [18–21, 24, 25]

Corrosion rate propagation model	Advantages/disadvantages	Trend
Breysse et al. model $\ln(i_{corr}) = 0.0312\text{RH} - 4736/T + 1.695\text{wc} - 0.391e + 14.589$	• Accounts for ambient conditions, quality of concrete mix and crosssection geometry • Requires availability of all input parameters at all times for accurate prediction	Constant
Yalcyn and Ergun's model $i_{corr}(t) = i_{corr}(1) \times e^{-\alpha t}$	• Model developed based on a time span of days and does not apply for long periods of time	Decreasing
Liu and Weyer's model $i_{corr}(t) = 102.47 + 10.09\ln(1.69\text{Cl}) - 39{,}038.96/T - 0.0015\Omega + 290.91t^{-0.215}$	• Accounts for ambient conditions and quality of concrete mix • Requires availability of all input parameters at all times for accurate prediction	Decreasing
Vu and Stewart's model $i_{corr}(t) = i_{corr}(1) \times \alpha t^{\beta}$ where $i_{corr}(1) = \frac{37.8(1-\text{wc})^{-1.64}}{e}$	• Implicitly accounts for quality of concrete mix and cross section geometry • Depending on the values of α and β, this model can simulate a stationary or time decreasing trend	Decreasing/constant
Li's model $i_{corr}(t) = 0.3686\ln(t) + 1.1305$	• Based on accelerated natural spraying corrosive conditions	Increasing

Where in all the above equations i_{corr} is the corrosion rate in $\mu A/cm^2$, RH is the relative humidity, T is the temperature at the steel level in Kelvin, wc is the water to cement ratio, e is the concrete cover depth in cm, Cl is the total chloride content at the steel level (kg/m^3), Ω is the resistivity of the concrete, α and β are empirical constants, and t is the corrosion time models is based on impressed currents which do not properly represent the heterogeneous nature of the corrosion propagation process [18–21, 24, 25].

In this study, representative corrosion propagation models are selected to be calibrated using experimental data. The selected models represent the different approaches commonly adopted for simulating long-term corrosion behavior: time decreasing, time increasing and stationary. The models that will be used in this study are:

The Vu and Stewart model as either a stationary or time-decreasing corrosion propagation model depending on the values adopted for α and β [20, 21]:

$$i_{\mathrm{corr}}(t) = i_{\mathrm{corr}(1)} \alpha t_{\mathrm{p}}^{\beta} \tag{1}$$

where t_{p} is the elapsed time post corrosion initiation and $i_{\mathrm{corr}(1)}$ is the initiation corrosion rate in μA/cm^2.

The Li corrosion propagation model [25] is a time-variant increasing model based on accelerated natural spraying corrosive conditions:

$$i_{\mathrm{corr}}(t) = C_A \ln(t) + C_B \tag{2}$$

where C_A and C_B are experimentally fitted parameters.

Real time data is used to calibrate the model parameters of the above corrosion propagation models and to identify the most suitable predictive model that properly simulates the L.M.D.C. experimental conditions.

3 Effect of corrosion on RC structures

The corrosion effects on the behavior of RC members can be observed in terms of loss of rebar cross sectional area and/or degradation of adhesion at the interface between the reinforcing bars and the surrounding concrete material. When corrosion initiates, a loss of rebar area immediately follows. As corrosion propagates, a progressive loss in the bond strength between the concrete and steel interface is observed.

Loss of cross-sectional area due tos corrosion can occur in two ways: either generalized with uniform pitting, mainly due to impressed simulated currents, or localized with spatial variability in pitting, a representation of the real corrosion phenomena. The corrosion penetration depth, often referred to as pitting depth, is calculated as [24]:

$$p(t) = \int 0.0116\, R_{\mathrm{pit}} i_{\mathrm{corr}}(t) \mathrm{d}t \tag{3}$$

where $p(t)$ is the pit depth in mm, R_{pit} is the ratio between pitting and uniform corrosion depths usually varying between 4 and 8 with a mean of 5.65, i_{corr} is the corrosion rate in μA/cm^2, and t is the time in years.

From the pitting depth, the relative loss of area of steel is calculated as follows [33]:

$$\Delta_w(t) = \left(1 - \frac{d_{\mathrm{b,remaining}}(t)^2}{d_{\mathrm{b,0}}^2}\right) \times 100 \tag{4}$$

where

$$d_{\mathrm{b,remaining}}(t) = d_{\mathrm{b,0}} - p(t) \tag{5}$$

and $d_{\mathrm{b,0}}$ is the initial bar diameter in mm, and $d_{\mathrm{b,remaining}}$ is the bar diameter at any time t.

Moreover, studies have shown that corrosion of RC structures is responsible for the decrease in bond strength between the reinforcement bars and the surrounding concrete. This loss in bond causes additional slippage of the reinforcement bars consequently leading to the failure of the structure. In this study, the model for the deterioration of bond strength developed by Lee et al. is used [34, 35]:

$$u_{\mathrm{b}} = 5.21 e^{-\Omega \Delta_w} \tag{6}$$

where u_{b} is the bond strength in MPa, Δ_w is the percentage steel area loss due to corrosion, and Ω is a fitting parameter shown to be equal to $-$ 0.0561 in Lee et al.'s study.

3.1 Excessive deflection

One measurable aspect of the effects of corrosion on RC structures is the increase in deflection. This increase in deflection results from the combined effects of the loss in tensile rebar area and the additional slippage of reinforcement bars caused by the loss in bond strength [29].

The loss in tensile rebar area leads to the degradation of the effective moment of inertia of the RC member and consequently to an excessive deflection as the latter is inversely proportional to the flexural stiffness of the cross-section.

Moreover, deflection is also dependent on slippage of reinforcement bars. This slippage is tied to the amount of rotational settlement θ_{s} which is significantly dependent on the corrosion state and is calculated as [35, 36]:

$$\theta_s = \frac{\varepsilon_s f_s d_b}{8u_b(d-c)} \quad \text{for} \ \ \varepsilon_s \leq \varepsilon_y \tag{7}$$

or

$$\theta_s = \frac{d_b}{8u_b(d-c)}\left(\varepsilon_y f_y + 2(\varepsilon_s + \varepsilon_y)(f_s - f_y)\right) \quad \text{for} \ \ \varepsilon_s > \varepsilon_y \tag{8}$$

where d_b is the tensile steel bar diameter, d is the effective depth of the beam, c is the depth of the neutral axis, ε_s is the steel strain, ε_y is the steel yield strain, f_s is the steel stress and f_y is the steel yield stress.

For instance, for a simply supported beam loaded at mid-span with point load P_{load}, the mid-span deflection is [37]:

$$\partial_{total} = \frac{P_{load} * L^3}{48E_c I_e} + \frac{\theta_s L}{4} \tag{9}$$

where I_e is the effective moment of inertia, L is the beam's length and E_c is the concrete's modulus of elasticity.

3.2 Corrosive crack width increase

Flexural loads cause transverse cracks to appear in beams. However, corrosion, engendering a loss of cross sectional area, is responsible for the longitudinal cracks that are present in cracking maps. These cracks are parallel to the rebar direction and constitute another measureable aspect of corrosion [6].

Vidal et al. developed an empirical cracking model to predict the propagation of corrosion by monitoring crack width [6].

$$w = K(\Delta A_s - \Delta A_{s0}) \tag{10}$$

where w is the crack width opening in mm, ΔA_s is the steel loss of cross-section in mm^2, ΔA_{s0} is the steel loss of cross-section at crack initiation in mm^2 and $K = 0.0575$ is a constant factor. $\Delta A_s(t)$ is computed as:

$$\Delta A_s(t) = A_{s0}\left[1 - \left[1 - \frac{R_{pit}}{d_b(t)}\left(7.53 + 9.32\frac{e}{d_b(t)}\right) \times 10^{-3}\right]^2\right] \tag{11}$$

where d_b is the remaining bar diameter (mm), R_{pit} is the pitting factor, e is the concrete cover (mm), and A_{s0} is the initial steel cross-section (mm^2).

4 Sequential data assimilation

Estimation theory uses statistical approaches where two inputs are provided and then combined into a weighted average. The first input is observed or measured data and the second is predicted based on governing system dynamics [38]. One of the most commonly used tools in estimation theory is the Kalman Filter. The Kalman Filter is an optimal filter for linear range dynamics and Gaussian error statistics only [4, 28]. The Kalman filter provides a linear, unbiased, minimum variance algorithm to estimate the state of a system from noisy measurements. For nonlinear dynamics or non-Gaussian perturbations, the Kalman Filter is no longer applicable and consequently, the ensemble Kalman filter (EnKF), an extension of the original Kalman Filter, can be used. The EnKF is based on forecasting the error statistics using Monte Carlo sampling. The EnKF propagates an ensemble of state vectors forward in time and updates the different realizations of the state vector as measurements become available. The initial ensemble is chosen so that it properly represents the error statistics of the initial guess of the model states. The initial ensemble is typically created by adding some kind of perturbation to a best-guess estimate, and then the ensemble is integrated over a time interval covering a few characteristic time scales of the dynamical system.

In the forecast stage, the mathematical model for corrosion propagation is presented as:

$$\mathbf{U_t} = f(\mathbf{U_{t-1}}) + \epsilon_\mathbf{t} \tag{12}$$

where $\mathbf{U}$ is a realization of the model state vector, f is the mathematical representation of the corrosion propagation model, t represents the time measure, and $\epsilon_\mathbf{t}$ is a zero mean random noise representing the model error at time t.

Whenever measurement data is available, a posterior estimate of each of the ensemble of forecasted state vectors is obtained as a linear combination of the a priori state, the available measurements, and the model predictions. The ensemble of state vectors is related to the measurement variables via an observation matrix **H** that selects forecasted values corresponding to the measurement locations from the state vectors. It is important to note that while a linear measurement operator is used in this application, the EnKF allows for nonlinear mapping between the model state vector and measurement data [39].

A new ensemble of observations is generated at each update step. The ensemble of observations is generated by adding perturbations with zero mean and covariance equal to the measurement error covariance matrix to the observation vector at time, *t*.

The updated states are computed as:

$$\mathbf{U}^{\mathbf{a}}_{\mathbf{t,i}} = \mathbf{U}^{\mathbf{f}}_{\mathbf{t,i}} + \mathbf{K_t}\left(\mathbf{d}_{\mathbf{t},l} - \mathbf{HU}^{\mathbf{f}}_{\mathbf{t,i}}\right) \quad \text{for } i = 1 \text{ to } \#\text{of ensembles} \tag{13}$$

where $U^a_{t,i}$ is the updated state vector at time t corresponding to the ith ensemble of the forecasted state vector, $U^f_{t,i}$.

$\mathbf{K_t}$ is called the Kalman Gain matrix and is given by,

$$\mathbf{K_t} = \mathbf{P_e H^T}\left(\mathbf{HP_eH^T} + \mathbf{R_e}\right)^{-1} \tag{14}$$

and the superscripts f and a denote the forecast and analysis stages respectively, $\mathbf{d_{t_i}}$ is a realization of the observation vector at time t, and $\mathbf{P_e}$ and $\mathbf{R_e}$ are the model and measurement covariance matrices respectively. Once the probabilistic characteristics of the model parameters are calibrated, they are used to predict the corrosion propagation rate and consequently better estimate the remaining service life of the structure.

5 Numerical validation

To validate the presented framework, the case study of an ongoing program of long-term chloride-induced corrosion experiments that was initiated in 1984 at "Laboratoire des Materiaux et Durabilite des Constructions" (L.M.D.C.) in Toulouse, south-west France is used. Data points pertinent to both deflection and crack width are gathered [29–31] from two beams subject to intense corrosive conditions and kept under constant supervision for a long period of time: 23 year old B2Cl1 [30] and 26 year old B2Cl2 [31].

Each of the two beams B2Cl1 and B2Cl2 was elastically loaded using a three point bending setup at sporadic time intervals, and the mid-span deflections were recorded. Two un-corroded control beams were subjected to the same loading conditions for comparative purposes [29]. The study showed that the mid-span deflections of the control non-corroded beams stabilize after 14 years indicating that the effects of the time-dependent material properties have vanished [29]. As a result, the mid-span deflections for the beams B2Cl1 and B2Cl2 at corrosion initiation can be considered equal to those of their respective control beams [30].

The data recorded beyond 17 years for B2Cl2 and beyond 19 years for B2Cl1 did not show a significant change in mid-span deflection measurements although the beams were still subject to the same corrosive conditions [30]. This is due to the fact that the steel–concrete bond is almost completely lost and generalized corrosion became stable. In fact, general attack corrosion occurs uniformly without appreciable localization, leading to relatively uniform thinning of the steel bar. At this stage, deflection being influenced by generalized corrosion loses its capacity to predict corrosion extent [40].

Moreover, the cracking maps of beams B2Cl2 and B2Cl1 were recorded in the literature at different time stages after corrosion initiation [29, 30, 40]. In this study, corrosion cracks on the tension surface only are considered. The averaged crack widths are tracked with time and recorded.

During the cracking stage, the behavior of corrosion leading to the heterogeneous formation of cracks is localized [40], and thus the pitting factor used should take the spatial variability into consideration. The latter is due to localized corrosion occurring at discrete sites on the steel bar surface.

6 Uncertainty quantification

Model-based predictions employ mathematical and empirical formulations to improve and demonstrate the knowledge of a certain phenomenon using numerical quantification [41]. However, these numerical models are not fully capable of simulating the exact status-quo. For this reason, the quantification of these model uncertainties is necessary to better simulate the naturally occurring phenomena. Moreover, uncertainties also exist in measured data typically used in the update stage of data assimilation frameworks. This section aims at numerically quantifying the different sources of uncertainties that liaise the corrosion propagation system identification framework.

6.1 Model uncertainties

More than one numerical model is involved in simulating the deflection and crack width responses of corroded structures.

6.1.1 Deflection model error

To quantify the error in the adopted slippage reinforcement model, the experimental data presented in the Lee et al. [34] experimental investigation is used. Figure 1 shows the comparison between the experimental data points (hollow circles) and a curve simulating the loss in bond strength as a function of the percentage loss in cross sectional area using Eq. (6) with $\Omega = -0.0561$. Moreover, Fig. 1 presents data labels corresponding to the estimated percent difference between the simulated and experimental data at different instants. The average residual error from all data points is found to be 16%. This error is consequently used to represent the modeling uncertainty associated with the reduction in bond strength model. It is important to note that in adopting this methodology, all measurement errors are disregarded and the hollow circles are assumed to represent the true state of the system. Equation (6) then becomes:

$$u_{\mathrm{b}} = 5.21 e^{-\Omega \Delta_w} + \epsilon_u \tag{15}$$

where ϵ_u is a normal distribution error with zero mean and an estimated standard deviation of 16% of the mean of u_{b}.

Manusco and Bartlett [42] found that an average error of approximately 24% represents the modeling uncertainty associated with calculating the effective moment of inertia using the Branson's equation. The equation for calculating the moment of inertia then becomes:

$$I_{\mathrm{e}} = \left(\frac{M_{\mathrm{cr}}}{M_{\mathrm{a}}}\right)^3 I_{\mathrm{g}} + \left[1 - \left(\frac{M_{\mathrm{cr}}}{M_{\mathrm{a}}}\right)^3\right] I_{\mathrm{cr}} + \epsilon_I \tag{16}$$

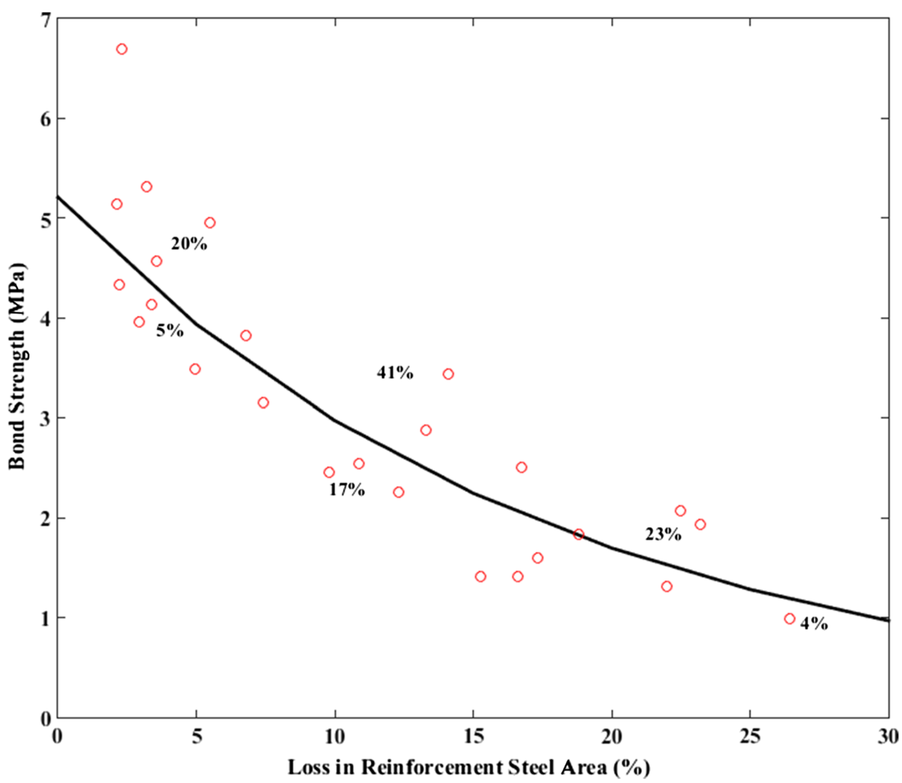

Fig. 1 Error quantification for the predictive model used for bond strength loss in RC members due to corrosion

where ϵ_I is a normal distribution error with zero mean and an estimated standard deviation of 24% of the mean of I_e, M_{cr} is the cracking moment, M_a is the applied moment, I_g is the gross moment of inertia and I_{cr} is the cracked moment of inertia.

In order to quantify the error associated with the deflection calculation, a Monte Carlo simulation was conducted using the errors corresponding to the slip model and to the effective moment of inertia model as presented in Eqs. (15) and (16) respectively. The resulting total average error for the deflection is found to be normal with a COV of 20%.

Therefore the total deflection equation becomes:

$$\partial_{\text{total}} = \partial_{\text{total}} + \epsilon_d \tag{17}$$

where ϵ_d is a normal distribution error with zero mean and an estimated standard deviation of 20% of the mean of ∂_{total}.

6.1.2 *Average corrosive crack width model error*

In order to quantify the model error associated with estimating the average corrosive crack width, the experimental data presented in the Vidal et al. [6] study is used. Figure 2 shows the comparison between the experimental data points (hollow circles) and a line simulating the corrosive crack mouth opening as a function of the change in percentage loss of cross sectional area using Eq. (10) with $K = 0.0575$. Moreover, Fig. 2 presents data labels corresponding to the estimated percent difference between the simulated and experimental data at different instants. The average error for all data points is found to be 19%. Therefore, Eq. (10) becomes:

$$w = K(\Delta A_s - \Delta A_{s0}) + \epsilon_c \tag{18}$$

where ϵ_c is a normal distribution error with zero mean and an estimated standard deviation of 19% of the mean of w.

6.1.3 *Corrosion propagation model error*

For the corrosion current propagation models, a zero mean Gaussian noise having a standard deviation of 20% of the mean of i_{corr} is used. The adopted corrosion propagation model error has been extensively used throughout the literature [20, 21, 25].

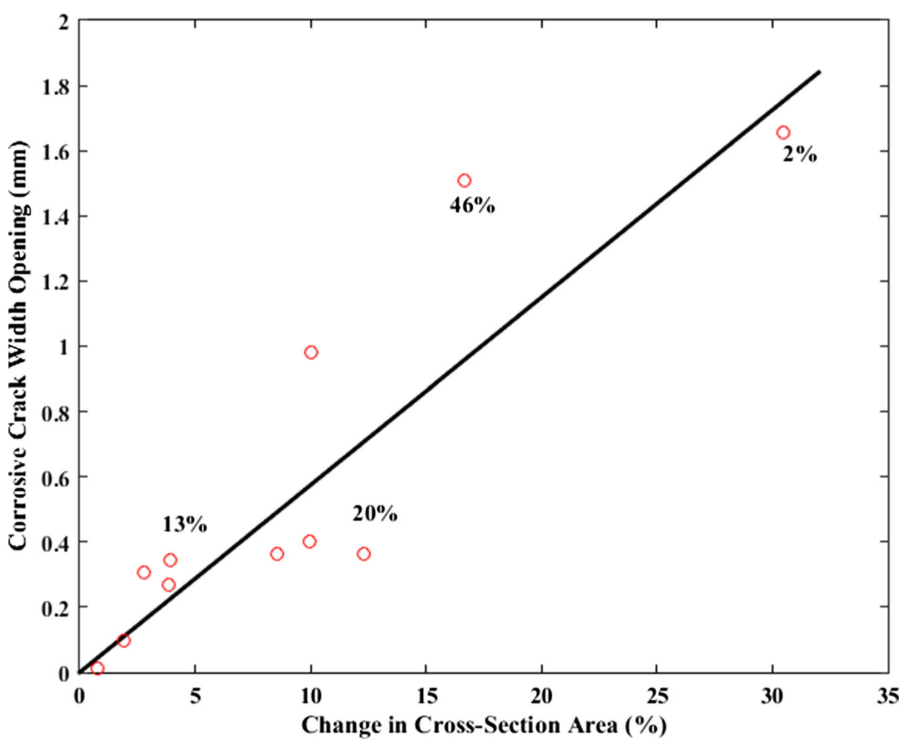

Fig. 2 Error quantification for the predictive model used for simulating corrosive crack width opening

6.2 Measurement error

The mid-span deflection and the crack width opening are the two measured parameters. Since both the deflection and the crack width are measured to the nearest 1/10 mm [29], an average error of 5% is associated to each to account for both the instrumentation error and the spatial variability of the response along the specimen.

7 EnKF formulation

The choice of three different empirical models to simulate the corrosion propagation rate requires three independent EnKF formulations. Each of these formulations will start with a stochastic state vector **U** representing the respective model state and parameters. Realizations of the state vector are then propagated forward in time using the governing dynamical equations as discussed earlier.

For each of the simulated cases, each realization of the state vector is represented as:

$$\mathbf{U_t} = [\mathbf{S} \;\; \mathbf{P} \;\; \mathbf{D} \;\; \mathbf{W}]^T \tag{19}$$

where $\mathbf{U_t}$ is a realization of the model state vector at time t, **S** is the state vector containing the mid-span deflection and the average corrosive crack width at time t, **P** is the vector containing the corrosion propagation model parameters, **D** is the vector containing the bond-slip deflection model parameters and **W** is the vector containing the crack width model parameters.

Of all the component of $\mathbf{U_t}$ shown in Eq. (19), only vector **P** changes depending on the choice of the corrosion propagation model.

Sub vector **S** is given by:

$$\mathbf{S} = [w \;\; \partial]^T \tag{20}$$

where w is the average corrosive crack width at time t and ∂ is the mid-span deflection at time t. The initializing parameters of sub vector **S** are the measured responses at corrosion initiating time, t = 5 years. Since these parameters are initially measured and not guessed, an initial zero mean Gaussian error having a COV of 5% is assigned to each of the two parameters. Furthermore, numerical checks are implemented to guarantee non negative values of deflection and crack width.

Sub vector **D** is represented as:

$$\mathbf{D} = \left[R_{\text{pit1}} \;\; d_{\text{b1}} \;\; \Omega\right]^T \tag{21}$$

where R_{pit1} is the generalized pitting factor associated with deflection. Throughout the literature, this parameter is taken as a deterministic value varying between 2 and 4 [33]. For this study, R_{pit1} is initially represented by a bounded normal distribution between 2 and 4 with a mean of 3 and a COV of 10%. d_{b1} is the steel bar diameter associated with generalized corrosion. Due to possible manufacturing errors, its initial guess is given a normal distribution with a COV of 3% [27]. Ω is the bond-slip model parameter. Since this parameter is uncertain, it is initialized as a normal distribution with a mean of − 0.0561 and a COV of 10%. The COV is limited to 10% since this parameter is based on the fitting of experimental data, and thus the update range should be narrowed.

Sub vector **W** is defined as:

$$\mathbf{W} = \left[R_{\text{pit2}} \;\; d_{\text{b2}} \;\; K\right]^T \tag{22}$$

where R_{pit2} is the localized pitting factor associated with crack width opening, having an initial Gumbel distribution truncated at 1 [27]. d_{b2} is the steel bar diameter associated with localized corrosion. Similar to d_{b1}, its initial guess is given a normal distribution with a COV of 3%. K is the crack-width model parameter initially represented via as a normal distribution with a mean of 0.0575 and a COV of 10%.

Vector **P** changes depending on the corrosion propagation model used in the analysis.

For the time-decreasing propagation model:

$$\mathbf{P} = \left[i_{\text{corr}(1)} \;\; \alpha \;\; \beta\right]^T \tag{23}$$

where $i_{\text{corr}(1)}$ is the initiation current propagation model parameter. Since this is a case of high corrosion, the initiation current should vary between 1 and 10 μA/cm^2 [32]. Due to this relative high range of possible values, this parameter is given an initial lognormal distribution with a COV of 60%. α and β are the two other model parameters for the time decreasing model, and are given initial guesses that are normal with a COV of 25%.

For the time-constant propagation model:

$$\mathbf{P} = \left[i_{\mathrm{corr}(1)}\right]^T \tag{24}$$

Similar to the time-decreasing propagation model, this parameter is given an initial lognormal distribution with a COV of 60%.

For the time-increasing propagation model:

$$\mathbf{P} = [C_A \quad C_B]^T \tag{25}$$

C_A and C_B are the two model parameters for the time-increasing propagation model, and are given uncertain initial guesses that are normal with a COV of 25%.

It is worthwhile to note that the initial COVs of α, β, C_A, and C_B are set based on a sensitivity analysis that investigated the effects of different ranges of initial guesses on the EnKF framework efficiency. Moreover, all distributions are truncated at zero to ensure meaningful sampling.

8 Results and discussions

The same set of measurement data is used to update the model parameters of the three different corrosion propagation rate models using the EnKF framework. Starting with an arbitrary mean initial guess for the state vectors corresponding to each of the two beams, measurements of the average corrosive crack width and the mid-span deflection are used to update the model parameters when available. After each update, the newly obtained model parameters are employed to forecast the crack width and deflection starting from corrosion initiation time.

8.1 Effect of the ensemble size

To study the sensitivity of the framework to the ensemble size, the consistency of the results when starting from different initial guesses for the state vector is investigated. To that extent, for every ensemble size, the simulation is run 100 times with different combinations of initial guesses. Figures 3 and 4 show the percent deviation of the average mean forecast results of the 100 simulations for each ensemble size from the case of an ensemble size of 200,000. The latter is assumed to simulate the true state. Figure 3 shows the results corresponding to the corrosive crack width opening for beam B2Cl2 while Fig. 4 shows the results for mid-span deflection for the same beam. It is important to note that the presented results are based on a forecast using the updated model parameters of the time increasing corrosion propagation model based on all available measurement data. Figure 3 shows that the error in estimating the average crack width for all 4 years considerably drops with the increase in ensemble size. For instance, the error in forecasting the average crack width at 17 years drops from 31% based on an ensemble size of 1000 to 3% when the ensemble size is increased to 20,000.

Similarly, Fig. 4 shows that the error in forecasting the mean mid-span deflection at 17 years drops from 93% based on an ensemble size of 1000 to 5% when the ensemble size is increased to 20,000. Consequently, it is decided to use an ensemble size of 20,000 for the rest of the simulations in this study.

8.2 Effect of number of updates

Figures 5, 6 and 7 show the forecast of the mean mid-span deflection and the mean average crack width as compared to measured data. In these figures the circles represent the measured data points, while each of the lines represents a mean forecast based on specific model parameters. For instance, the dotted lines represent the mean simulated results using the initial guess parameters only without relying on any measurement data. On the other hand, the solid lines are forecasts based on updated model parameters using all available measurement points. Moreover, Error bars representing one standard deviation away from the mean are also shown on the figures for the final updated model parameters' mean prediction only.

For all the presented results, time 0 refers to the onset of corrosion, in this case at 5 years from the starting point of the experiment [29]. For illustration purposes, only the results of beam B2Cl2 will be showcased first and then the results for both beams will be summarized.

8.2.1 *Time-decreasing model*

For the corrosion rate time-decreasing model, Fig. 5 shows the forecast of the mid-span deflection and average crack width as compared to measured data for beam B2Cl2.

As indicated earlier, the only part of the state vector that is varied from one model to another is that pertaining to the corrosion propagation model

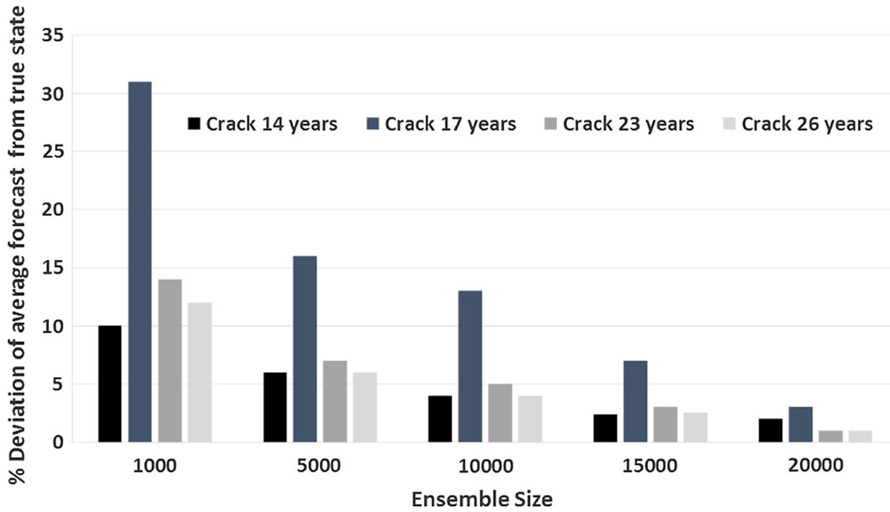

Fig. 3 Error in estimating average corrosive crack width as a function of ensemble size for beam B2Cl2

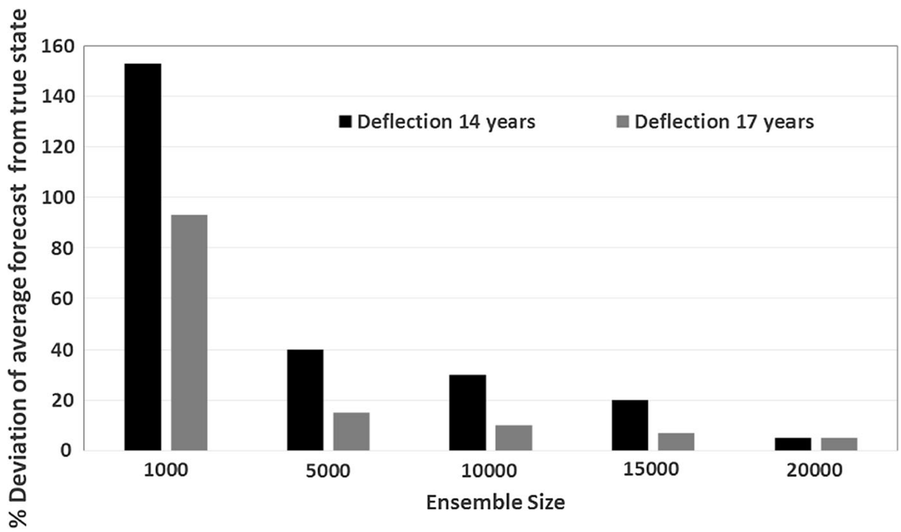

Fig. 4 Error in estimating the mean mid-span deflection as a function of ensemble size for beam B2Cl2

adopted. Table 2 shows the probabilistic characterization for the initial guess of the augmented model state vector corresponding to beam B2Cl2.

Starting with this initial guess, the progression of the mean crack width and mid-span deflection increase are forecasted according to the dotted line in Fig. 5. The figure shows that the initial model parameters underestimate the corrosion extent for beam B2Cl2, falling well below the measured points. Once the first measurement data set is made available, and the model parameters are updated using the EnKF framework, the dash-dotted lines in Fig. 5 depict the new mean forecast of the crack width and mid-span deflection starting from time 0 and using the updated model parameters. Although the dash-dotted lines show local improvements in forecasting the state of the beams at $t = 9$ years (time of update), the global forecasted response diverges implying that the updated parameters based on one measurement only cannot capture the true behavior of the corroded specimens.

As the second set of measurement data is made available, the once updated model state vector undergoes another update stage. The forecast using the newly updated parameters represented using the '+' line for the crack width and a solid line for deflection is a more accurate representation of the actual state of corrosion than the preceding forecasts.

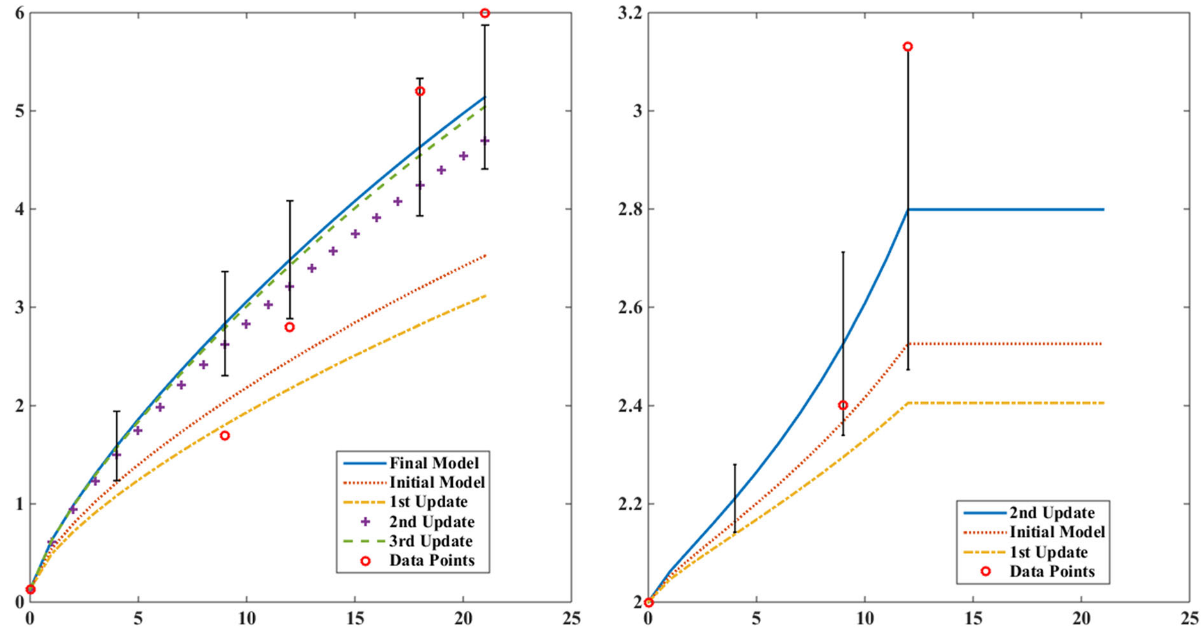

Fig. 5 B2Cl2 time-decreasing model: **a** corrosive crack width; **b** mid-span deflection

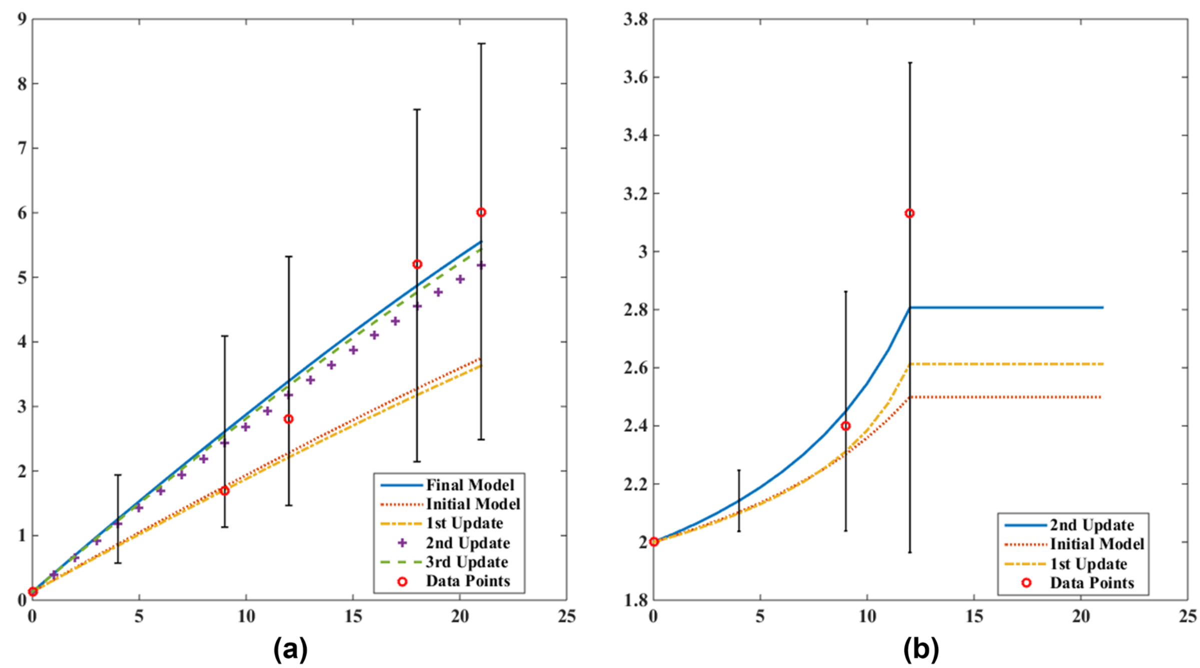

Fig. 6 B2Cl2 time-constant model: **a** corrosive crack width; **b** mid-span deflection

For the deflection, this update is the final update, and therefore error bars at one standard deviation away from the mean are shown on the plots. Although, a limited number of measurement points is available for deflection, the presented framework using the time-decreasing model is shown capable of forecasting a mean final deflection within one standard deviation away from the true state for beam B2Cl2.

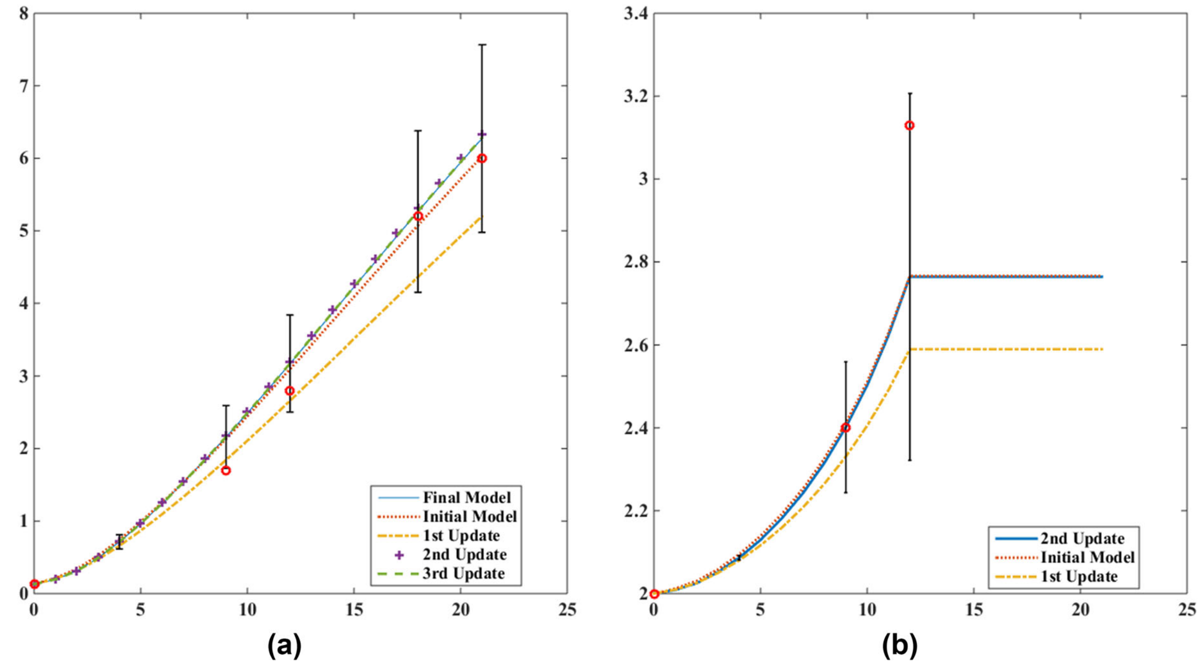

Fig. 7 B2Cl2 time-increasing model: **a** corrosive crack width; **b** mid-span deflection

Table 2 Time-decreasing corrosion propagation model state vector

Time-decreasing corrosion propagation model			
State vector parameter	Distribution type	Mean	Covariance (%)
w	Normal truncated at zero	0.13	5
δ	Normal truncated at zero	0.002	5
i_{corr1}	Lognormal	2.75	60
α	Normal truncated at zero	0.85	25
β	Normal truncated at zero	− 0.29	25
R_{pit1}	Normal bounded between 2 and 4	3	10
d_{b1}	Normal truncated at zero	0.012	3
Ω	Normal	− 0.0561	10
R_{pit2}	Gumbel truncated at 1	5.65	20
d_{b2}	Normal truncated at zero	0.012	3
K	Normal truncated at zero	0.0575	10

As more data points are made available for the crack width, the incremental improvement in the forecasted state as shown in Fig. 5 becomes less significant. The third and fourth (final) updates oscillate around the 2nd update with limited/no significant improvement in the forecasted state. The forecast state based on the final update of the corrosive crack width for B2Cl2 shows that the error in the mean predictions at 9, 12, 18 and 21 years change from 22%, 11%, 38%, and 42% to 66%, 17%, 11% and 14% respectively as compared to the initial model prediction. Although the time decreasing model with the final updated parameters succeeds in reducing the error in the predictions for times of 12 years and later, it fails in properly predicting the crack width at 9 years showing some limitations of the adopted corrosion propagation model. It is to be noted that the reported error in the mean predictions is computed as a measure of the average distance between the predictions and the measurements. Furthermore, since this error is mainly used to evaluate the relative performance of the different models as a function of the number of available updates, the discrepancy measure used does not account for any possible errors in the observation data. Other works available in the literature introduce probabilistic formulations which take into account measurement errors for evaluating predictive accuracy [39, 43].

8.2.2 Time-constant model-robustness

For the time-constant corrosion propagation model, Fig. 6 shows the forecast of the mid-span deflection and average crack width as compared to measured data for beam B2Cl2.

Table 3 shows the probabilistic characterization for the initial guess of the augmented model state vector corresponding to beam B2Cl2.

Starting with this assumed initial guess, the progression of the mean crack width and deflection increase is forecasted according to the dotted line in Fig. 6. The results show that the time constant model fails in accurately predicting the final mean mid-span deflection as the error reported for the B2Cl2 estimate is relatively large.

As for the corrosive crack width, the third and final updates for beam B2Cl2 almost overlap with the first two updates, signifying the efficacy of the time constant model in simulating the crack width behavior of corroded beams even with a limited amount of measurement data. In fact, the forecast state based on the final update shows that the error in the mean prediction of average corrosive crack width at 9, 12, 18 and 21 years change from 4%, 18%, 38%, and 38% to 47%, 15%, 6% and 8% respectively as compared to the initial model prediction.

8.2.3 Time-increasing model-robustness

For the corrosion rate time-increasing model, Fig. 7 shows the forecast of the mid-span deflection and average crack width as compared to measured data for beam B2Cl2.

For the time increasing corrosion propagation model scenario, Table 4 shows the probabilistic characterization for the initial guess of the augmented model state vector corresponding to beam B2Cl2.

Similar to the time constant model, the time increasing model shows a poor performance in predicting the final mean mid-span deflection as the final reported error is relatively large.

As for the corrosive crack width, the time increasing model successfully captures the crack width behavior after the second update. This signifies the efficacy of the time increasing model in simulating the crack width behavior of corroded beams even with a limited amount of measurement data. The forecast state based on the final update shows that the error in the mean predictions of the average corrosive crack width at 9, 12, 18 and 21 years change from 13%, 2%, 10%, and 7% to 20%, 9%, 1% and 2% respectively as compared to the initial model predictions. As for the error in mean predictions of the mid-span deflection at 9 and 12 years, it changes from 2% and 16% to 1% and 12% respectively.

Table 3 Time-constant corrosion propagation model state vector

Time-constant corrosion propagation model			
State vector parameter	Distribution type	Mean	Covariance (%)
w	Normal truncated at zero	0.13	5
δ	Normal truncated at zero	0.002	5
i_{corr1}	Lognormal	1.5	60
R_{pit1}	Normal bounded between 2 and 4	3	10
d_{b1}	Normal truncated at zero	0.012	3
Ω	Normal	− 0.0561	10
R_{pit2}	Gumbel truncated at 1	5.65	20
d_{b2}	Normal truncated at zero	0.012	3
K	Normal truncated at zero	0.0575	10

Table 4 Time-increasing corrosion propagation model state vector

Time-increasing corrosion propagation model			
State vector parameter	Distribution type	Mean	Covariance (%)
w	Normal truncated at zero	0.13	5
δ	Normal truncated at zero	0.002	5
C_A	Normal truncated at zero	0.9	25
C_B	Normal truncated at zero	0.6686	25
R_{pit1}	Normal bounded between 2 and 4	3	10
d_{b1}	Normal truncated at zero	0.012	3
Ω	Normal	− 0.0561	10
R_{pit2}	Gumbel truncated at 1	5.65	20
d_{b2}	Normal truncated at zero	0.012	3
K	Normal truncated at zero	0.0575	10

8.3 Comparative analysis of all three models

To assess the sensitivity of the framework to different initial guesses and to better compare the performance of the three corrosion propagation models, a Monte Carlo simulation with 100 realizations of initial guesses is run through the EnKF framework with 20,000 ensembles for both beams B2Cl1 and B2Cl2.

For each simulation, the discrepancy between the simulated data and the available experimental data is recorded after each update. This error is computed as:

$$\%\text{error} = \sum_i \frac{u^i_{\text{measured}} - u^i_{\text{simulated}}}{u^i_{\text{measured}}} \times 100 \tag{26}$$

where i represents the number of available measurement data, u^i_{measured} is the measured variable (crack width or deflection) at time i, and $u^i_{\text{simulated}}$ is the corresponding simulated value of the measured variable.

Table 5 below presents the average of the errors computed for all 100 simulations. For instance, it shows the average error in computing the mean mid-span deflection and the average corrosive crack width opening after each update for the different initial guess realizations for Beam B2Cl1. For example, the presented data shows that the error using the time decreasing corrosion propagation model to predict the average corrosive crack width drops from 47% based on the initial guess propagation only to 14% when all available measurements are used for model calibration. The time decreasing model mid-span deflection prediction error also drops from 17 to 11.5% as more measurements become available. Based on these results presented in Table 5, the predictive accuracy of all three

Table 5 Average error for mid-span deflection and corrosive crack width for beam B2Cl1 and beam B2Cl2 respectively

# Updates	Average corrosive crack width prediction error (%)					Mid-span deflection prediction error (%)		
	0	1	2	3	4	0	1	2
Beam B2Cl1								
Average decreasing	46.7	17.2	15.0	13.8	N/A	16.9	12.8	11.4
Average constant	32.3	12.6	10.3	9.1	N/A	18.2	13.2	11.1
Average increasing	27.0	11.7	10.2	9.8	N/A	15.6	12.4	10.4
Beam B2Cl2								
Average decreasing	41.5	32.5	25.5	24.4	23.2	15.5	13.9	7.9
Average constant	39.1	29.4	25.4	23.5	22.8	16.0	10.3	7.8
Average increasing	22.9	16.9	12.9	12.7	11.7	12.1	10.1	7.3

corrosion propagation models significantly improved in simulating the mid-span deflection and the crack width opening for Beam B2Cl1.

Table 5 presents the errors for calculating the mid-span deflection and the crack width opening for Beam B2Cl2 as well. These results also confirm the previous conclusions deduced from the same table. However, for beam B2Cl2, the results show that the calibrated time increasing model has the highest accuracy in predicting the average crack width opening while all models have similar predictive accuracy when it comes to mid-span deflection.

9 Conclusions

This study presents a stochastic framework based on the implementation of the EnKF for accurate prediction of the extent of corrosion propagation and its effects on RC members. The main contributions of this study are summarized below:

- The study relies on a finite-difference numerical scheme to propel the dynamic process of corrosion in time, using a corrosion propagation model, a corrosive crack width model and a bond slip and flexural model for estimating deflection.
- The presented SHM framework is applied to a long-term experimental data set corresponding to the natural corrosion occurring process which is a first in the literature. The experimental program, naturally accelerated, accurately simulates real time corrosion unlike other experimental programs in the literature that simulate corrosion through impressed currents, a non-accurate representation of the heterogeneous distribution of corrosion.
- The presented SHM framework aims to update three different corrosion propagation models. The selection of these models was made since they represent three different approaches for simulating long-term corrosion propagation behavior: a time decreasing model, a time increasing model and a time constant model.
- The presented SHM framework calibrates the governing parameters of corrosion propagation models by simply monitoring easily measurable, non-costly and non-destructively tested aspects of corrosion, namely deflection and crack width opening.
- The reported results show that, once updated using the EnKF framework, all three types of corrosion propagation models are able to capture the experimental response with variable accuracy while significantly reducing the deviation between predicted and measured parameters with each update.
- The limitations of the framework are centered on the scarceness of the assembled data in the literature: only two beams' progresses were tracked through time. More corroded RC members should be studied in order to fully understand the progression of corrosion.

Acknowledgements The authors would like to acknowledge the University Research Board at the American University of Beirut for funding this study.

Compliance with ethical standards

Conflict of interest The authors certify that they have NO affiliations with or involvement in any organization or entity with any financial or non-financial interest in the subject matter or materials discussed in this manuscript.

References

1. Qiao G, Xiao H, Sun G (2011) Identification of the reinforcing steel's corrosion state in RC beams based on electrochemical sensor. Sens Rev 31:218–227
2. Koch GH, Brongers PH, Virmani YP, Payer J (2002) Corrosion costs and preventive strategies in the United States. NACE International, Houston
3. Tuutti K (1982) Corrosion of steel in concrete. Swedish Cement and Concrete Research Institute, Stockholm
4. Slika W, Saad G (2016) An ensemble Kalman filter approach for service life prediction of reinforced concrete structures subject to chloride-induced corrosion. Constr Build Mater 115:132–142
5. Siamphukdee K, Collins F, Zou R (2013) Sensitivity analysis of corrosion rate prediction models utilized for reinforced concrete affected by chloride. J Mater Eng Perform 22(6):1530–1540
6. Vidal T, Castel A, Francois R (2004) Analyzing crack width to predict corrosion in reinforced concrete. Cem Concr Res 34(1):165–174
7. Taha NA, Morsy M (2016) Study of the behavior of corroded steel bar and convenient method of repairing. HBRC J 12(2):107–113
8. Shayanfar M-A, Barkhordari M-A, Ghanooni-Bagha M (2015) Probability calculation of rebars corrosion in reinforced concrete using CSS algorithms. J Cent South Univ 22(8):3141–3150
9. Azad AK, Ahmad S, Azher SA (2007) Residual strength of corrosion-damaged reinforced concrete beams. ACI Mater J 104(1):40–47

10. Chung L, Paik IK, Cho S, Roh YS (2006) Infrared thermographic technique to measure corrosion in reinforcing bar. Key Eng Mater 321:821–824
11. Kobayashi K, Banthia N (2011) Corrosion detection in reinforced concrete using induction heating and infrared thermography. J Civ Struct Health Monit 1(2):25–35
12. Baek S, Xue W, Feng M, Kwon S (2012) Nondestructive corrosion detection in RC through integrated heat induction and IR thermography. J Nondestruct Eval 2(31):181–190
13. Akiyama M, Frangopol D (2012) Estimation of steel weight loss due to corrosion in RC members based on digital image processing of X-ray photogram. In: Proceedings of the 3rd international symposium on life-cycle civil engineering, Vienna, Austria
14. Itty P, Serdar M, Meral C, Parkinson D, MacDowell A, Bjegović D et al (2014) In situ 3D monitoring of corrosion on carbon steel and ferritic stainless steel embedded in cement paste. Corros Sci 83:409–418
15. Michel A, Pease B, Geiker M, Stang H, Olesen J (2011) Monitoring reinforcement corrosion and corrosion-induced cracking using non-destructive X-ray attenuation measurements. Cem Concr Res 41(11):1085–1094
16. Ahmad S, Bhattacharjee B (1995) A simple arrangement and procedure for in situ measurement of corrosion rate of rebar embedded in concrete. Corros Sci 37(5):781–791
17. Alghamdi S, Ahmad S (2014) Service life prediction of RC structures based on correlation between electrochemical and gravimetric reinforcement corrosion rates. Cem Concr Compos 8:47–94
18. Liu T, Weyers R (1998) Modeling the dynamic corrosion process in chloride contaminated concrete structures. Cem Concr Res 28(3):365–379
19. Yalcyn H, Ergun M (1996) The prediction of corrosion rates of reinforcing steels in concrete. Cem Concr Res 26(10):1593–1599
20. Vu KA, Stewart MG (2000) Structural reliability of concrete bridges including improved chloride-induced corrosion models. Struct Saf 22(4):313–333
21. Vu K, Stewart MG, Mullard J (2005) Corrosion-induced cracking: experimental data and predictive models. ACI Struct J 102(5):719
22. Alonso C, Andrade C, Gonzalez J (1988) Relation between resistivity and corrosion rate of reinforcements in carbonated mortar made with several cement types. Cem Concr Res 18(5):687–698
23. Otieno M, Beushausen H, Alexander M (2011) Prediction of corrosion rate in RC structures—a critical review. Modelling of corroding concrete structures, Springer, pp 15–37
24. El Hassan J, Bressolette P, Chateauneuf A, El Tawil K (2010) Reliability-based assessment of the effect of climatic conditions on the corrosion of RC structures subject to chloride ingress. Eng Struct 32(10):3279–3287
25. Li CQ, Lawanwisut W, Zheng J (2005) Time-dependent reliability method to assess the serviceability of corrosion-affected concrete structures. J Stuct Eng 131(11):1674–1680
26. Faroz SA, Pujari N, Ghosh S (2016) Reliability of a corroded RC beam based on Bayesian updating of the corrosion model. Eng Struct 126:457–468
27. Hackl J, Kohler J (2016) Reliability assessment of deteriorating reinforced concrete structures by representing the coupled effect of corrosion initiation and progression by Bayesian networks. Struct Saf 62:12–23
28. Evensen G (1994) Sequential data assimilation with a nonlinear quasi-geostrophic model using Monte Carlo methods to forecast error statistics. J Geophys Res Oceans 29(C5):10143–10162
29. Vidal T, Castel A, Francois R (2007) Corrosion process and structural performance of a 17 year old reinforced concrete beam stored in chloride environment. Cem Concr Res 37(11):1551–1561
30. Zhang R, Castel A, Francois R (2009) Serviceability limit state criteria based on steel–concrete bond loss for corroded reinforced concrete in chloride environment. Mater Struct 42(10):1407
31. Zhu W, Francois R (2014) Corrosion of the reinforcement and its influence on the residual structural performance of a 26-year-old corroded RC beam. Constr Build Mater 51:461–472
32. Otieno M, Alexander M, Beushausen H-D (2010) Corrosion in cracked and uncracked concrete—influence of crack width, concrete quality and crack reopening. Mag Concr Res 62(6):393–404
33. Zhu W, Francois R (2015) Structural performance of RC beams in relation with the corroded period in chloride environment. Mater Struct 48(6):1757–1769
34. Lee H-S, Cho Y-S (2009) Evaluation of the mechanical properties of steel reinforcement embedded in concrete specimen as a function of the degree of reinforcement corrosion. Int J Fract 157:81–88
35. Yalciner H, Sensoy S, Eren O (2012) Effect of corrosion damage on the performance level of a 25-year-old reinforced concrete building. Shock Vib 19(5):891–902
36. Moehle J (2014) Seismic design of reinforced concrete buildings. McGraw Hill Professional, New York
37. Soltis LA (1981) Analysis of continuous beams with joint slip. US Dept. of Agriculture, Forest Service, Forest Products Laboratory, Madison
38. Stroud JR, Katzfuss M, Wikle CK (2016) A Bayesian adaptive ensemble Kalman filter for sequential state and parameter estimation. arXiv preprint
39. Khalil M, Sarkar A, Adhikari S, Poirel D (2015) The estimation of time-invariant parameters of noisy nonlinear oscillatory systems. J Sound Vib 344:81–100
40. Zhang R, Castel A, Francois R (2009) The corrosion pattern of reinforcement and its influence on serviceability of reinforced concrete members in chloride environment. Cem Concr Res 39(11):1077–1086
41. Slika W, Saad G (2018) Probabilistic identification of chloride ingress in reinforced concrete structures: polynomial chaos Kalman filter approach with experimental verification. J Eng Mech 144(6):04018037
42. Mancuso C, Bartlett FM (2017) ACI 318-14 criteria for computing instantaneous deflections. ACI Struct J 114(5):1299
43. Bisaillon P, Sandhu R, Khalil M, Pettit C, Poirel D, Sarkar A (2015) Bayesian parameter estimation and model selection for strongly nonlinear dynamical systems. J Nonlinear Dyn 82:1061–1080